Spring-Like Pseudoelectroelasticity of Monocrystalline Cu₂S Nanowire

Qiubo Zhang,[†,‡,#] Zhe Shi,[§,#] Kuibo Yin,[†] Hui Dong,[†] Feng Xu,[†] Xinxing Peng,[‡] Kaihao Yu,[†] Hongtao Zhang,[†] Chia-Chin Chen,[∥] Ilia Valov,[*,⊥] Haimei Zheng,[*,‡,▽] and Litao Sun[*,†,○]

[†]SEU-FEI Nano-Pico Center, Key Laboratory of MEMS of Ministry of Education, Collaborative Innovation Center for Micro/Nano Fabrication, Device and System, Southeast University, Nanjing 210018, P. R. China

[‡]Materials Science Division, Lawrence Berkeley National Laboratory, Berkeley, California 94720, United States

[§]Department of Materials Science and Engineering, Massachusetts Institute of Technology, Cambridge, Massachusetts 02139, United States

[∥]Max Planck Institute for Solid State Research, Heisenbergstrasse 1, 70569 Stuttgart Germany

[⊥]Peter Gruenberg Institute, Electronic Materials, Research Centre Juelich, 52425 Juelich, Germany

[▽]Department of Materials Science and Engineering, University of California, Berkeley, California 94720, United States

[○]Center for Advanced Materials and Manufacture, Joint Research Institute of Southeast University and Monash University, Suzhou 215123, P. R. China

S *Supporting Information*

ABSTRACT: Prediction from the dual-phase nature of superionic conductors—both solid and liquid-like—is that mobile ions in the material may experience reversible extraction−reinsertion by an external electric field. However, this type of pseudoelectroelasticity has not been confirmed *in situ*, and no details on the microscopic mechanism are known. Here, we *in situ* monitor the pseudoelectroelasticity of monocrystalline Cu₂S nanowires (NWs) using transmission electron microscopy (TEM). Specifically, we reveal the atomic scale details including phase transformation, migration and redox reactions of Cu⁺ ions, nucleation, growth, as well as spontaneous shrinking of Cu protrusion. Caterpillar-diffusion-dominated deformation is confirmed by the high-resolution transmission electron microscopy (HRTEM) observation and *ab initio* calculation, which can be driven by either an external electric field or chemical potential difference. The observed spring-like behavior was creatively adopted for electric nanoactuators. Our findings are crucial to elucidate the mechanism of pseudoelectroelasticity and could potentially stimulate in-depth research into electrochemical and nanoelectromechanical systems.

KEYWORDS: *In situ TEM, pseudoelectroelasticity, Cu₂S nanowires, superionic conductors*
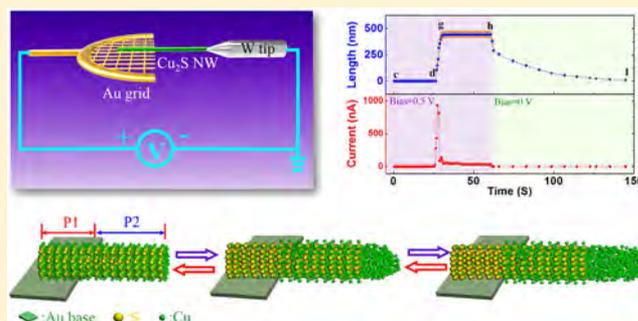
Superionic conductors possessing both rigid solid and fluidic liquid sublattices[1] can offer special applications in energy conversion,[2−5] memristive systems,[6,7] and crystal growth.[8] A characteristic feature of the dual-phase nature is that the mobile ions occupying the fluidic sublattice may be extracted out of their sublattice under an application of electric field, and be spontaneously reinserted into the material upon removal of the electrical bias, driven by chemical potential gradient. This process, known as "pseudo-electroelasticity", is essential for unveiling the microscopic working mechanisms responsible for various functional superionic conductors and remains challenging to identify and characterize experimentally.

Valuable work has been conducted to study the microscopic mechanism of redox reactions, ion transport, and mass transfer in various superionic conductors.[5−16] For example, Valov et al. studied the atomical nucleation at superionic solid electrolyte surface.[12] Ohno et al. studied the short-term plasticity and long-term potentiation in mixed electronic-superionic inorganic synapses.[6] Chen et al. studied the ultrafast silver mass storage and removal in mixed conductors.[5] However, a wide range of microscopic processes are so far still elusive including the diffusion of mobile species during the growth and dissolution processes of the metal protrusion is not evidently revealed,[12,13,17] the corresponding relation between measured total current and atoms/ions movement remains to be
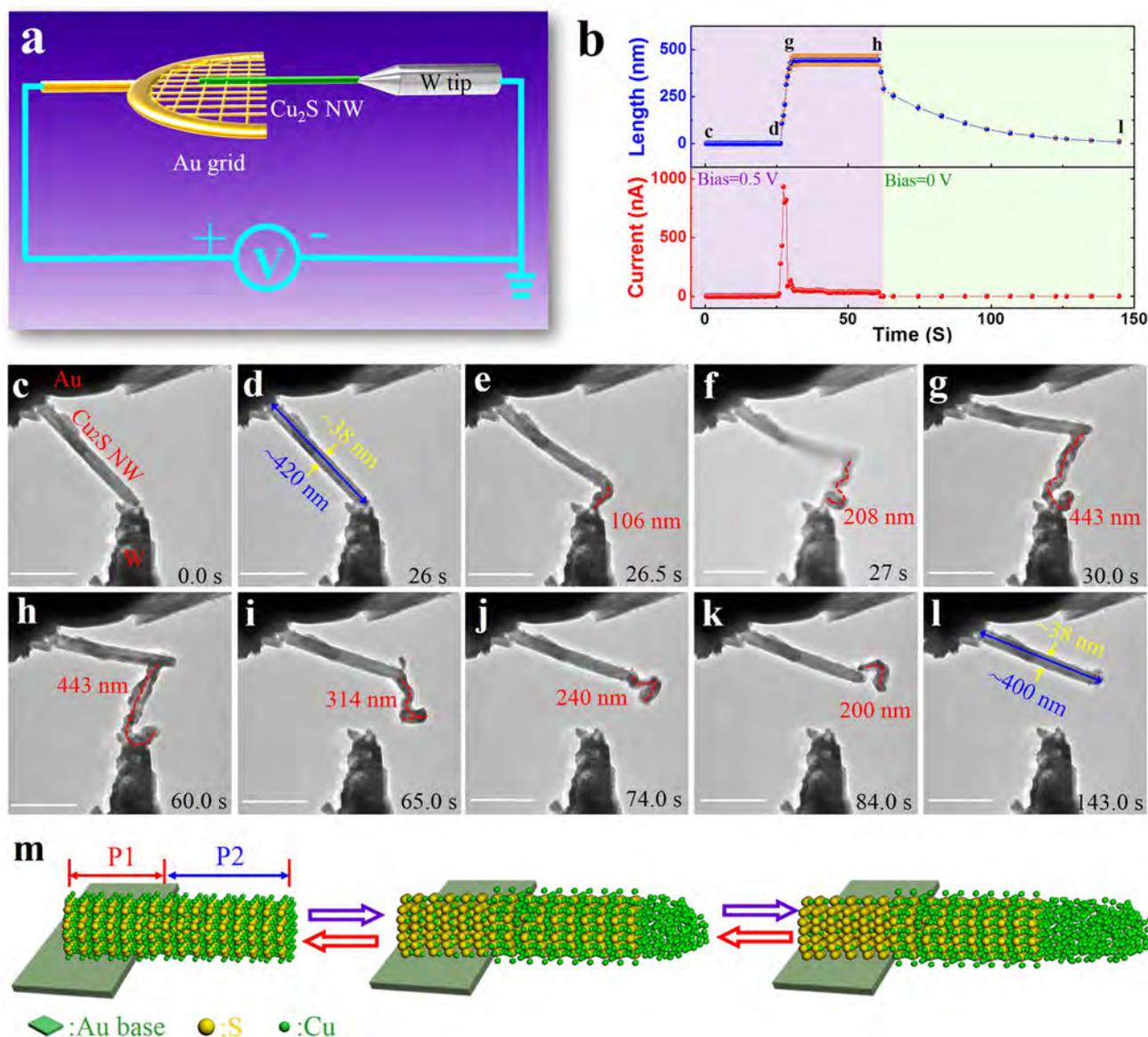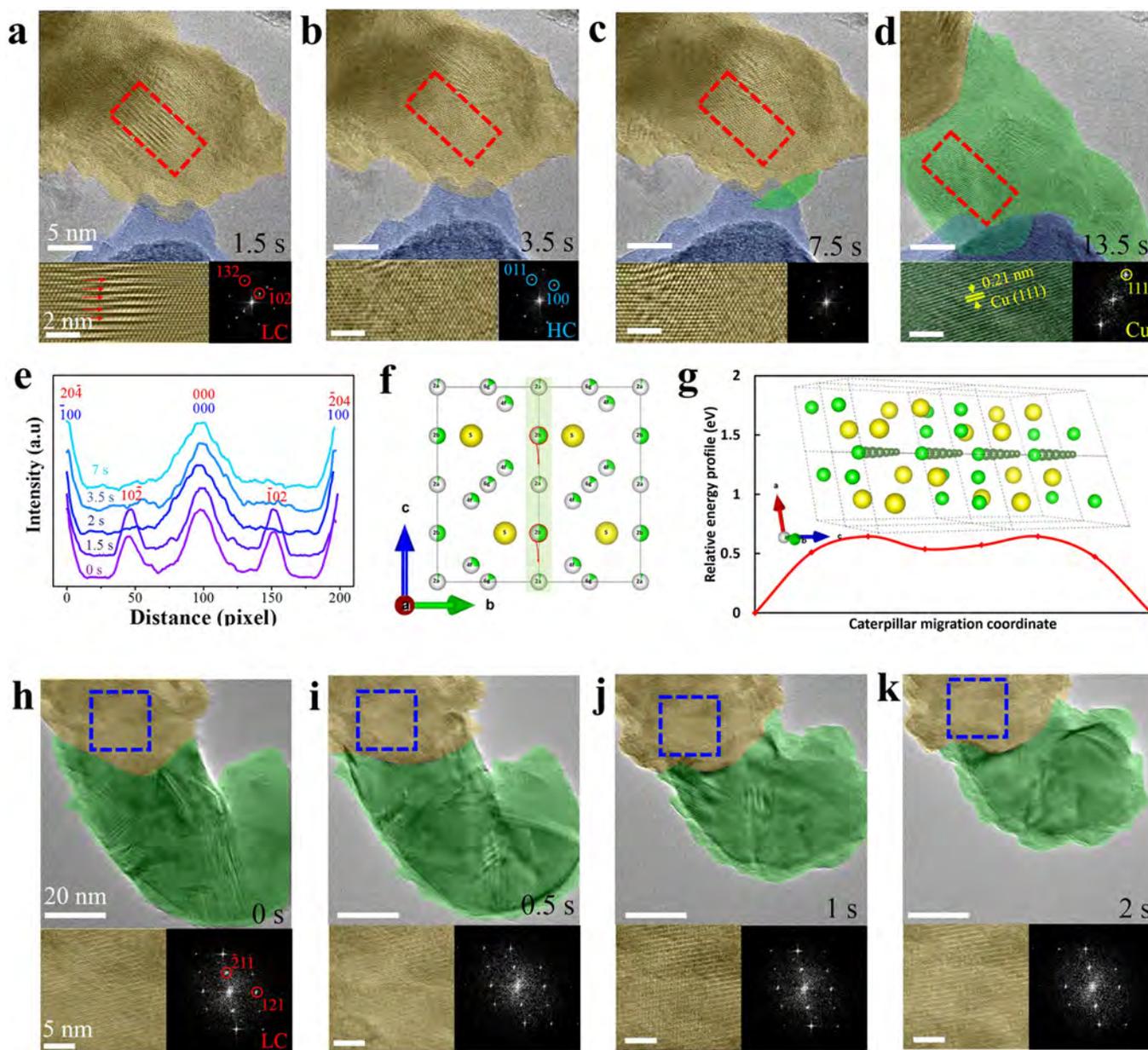
Figure 1. Pseudoelectroelasticity deformation of Cu_2S NWs. (a) Schematic illustration of the *in situ* experimental setup. In the experimental setup, the Cu_2S NW was supported on a half-Au grid and the other end contacted to a grounded W tip, both working as chemical inert electrodes. (b) Current vs time and length vs time curves are recorded during the pseudoelectroelasticity process. The applied voltage for ion extrusion is 0.5 V lasting 60 s and 0 V for the insertion process. Error bars indicate the standard deviation. (c−l) Snapshots of the pseudoelectroelasticity process demonstrating Cu protrusion growth and dissolution. The Cu_2S NW has an initial length of 420 nm (almost recovered with a final length of 400 nm) and diameter of 38 nm (unchanged). Scale bars, 200 nm. (m) Schematics of the extrusion and reinsertion process. The NW is divided into two parts: one part (P1) loaded on the gold grid acts as a Cu^+ ion reservoir and the other part projecting out of the grid (P2) is mainly used for the transmission of Cu^+ ions. During the extrusion process, the Cu^+ ions in P2 are driven out of their regular positions, while the Cu^+ ions in P1 migrate into P2 to fill the Cu^+ ion vacancies. The extruded Cu^+ ions are blocked/oxidized at the Cu_2S/W interface and are pushed forward by the new oxidized Cu atoms. During reinsertion process, the Cu^+ ions in P2 migrate back into P1 and following the extruded Cu^+ ions move back into P2. The blue and red arrows refer to the extrusion and reinsertion processes, respectively.

characterized,[14,17] and the long-term stability of protrusion after gap bridged is yet to be confirmed by imaging.[6,12,13]

One bottleneck of the *in situ* study of such process is the difficulty of facilitating ion transport pathways in typical materials. To alleviate this problem, the material system of monocrystalline Cu_2S nanocrystals came into our attention. Our previous work proved that the Cu_2S can be heat-treated to undergo a phase transformation from low chalcocite (LC) to high chalcocite (HC) near room temperature,[18,19] and the HC phase exhibits superionic properties with its S atoms forming a rigid sublattice and Cu atoms randomly jumping around

similar to a liquid.[1] This allows chemical potential gradient and external electric field to easily drive the mobilizing Cu^+ ions in and out of their sublattice, opening up a large window to observe pseudoelectroelasticity under an STM−TEM system. We were thus able to monitor the whole pseudoelectroelasticity process including LC-to-HC phase transformation, migration and jamming of Cu^+ ions, nucleation, and growth, as well as spontaneous shrinking of a Cu protrusion.

Results and Discussion. In our experiment, we constructed a close-circuit electrochemical system with a monocrystalline LC-phase Cu_2S NW (Figure S1) incorporated

Figure 2. Microstructure evolution of the NW during the pseudo electroelasticity process. (a−d) Top: TEM images of one Cu_2S NW during the extrusion process at different times; bottom: HRTEM images of the corresponding red dot square areas (left) and corresponding FFT patterns (right). (e) Line profiles of FFT patterns along the [100] direction of S sublattice ([$\bar{1}02$] direction of the LC or [100] direction of HC) showing phase evolution. (f) Atomic structure of HC phase Cu_2S. Four different Cu sites are marked in green, with the fraction of color showing the fractional occupancy of the respective site. Highlighted are the Cu atoms in the 2b site (the most probable site) participating in the c channel migration. (g) The energy landscape of concerted migration of Cu 2b atoms along the c channel (shown in inset). (h−k) Top: TEM images of one Cu_2S NW during the insertion process; bottom: HRTEM images of the corresponding blue dot square areas (left) and corresponding FFT patterns (right), with the Cu_2S, Cu protrusion, and W tip highlighted in gold, green, and blue, respectively. The weak contrast of the blue part in parts a−d is an amorphous carbon coating on the W tip, which does not influence the experiment.

between Au and W ends, as shown in Figure 1a. A bias was applied to induce NW pseudoelectroelasticity (Video S1). During the whole process, the loop current in the circuit as well as the length of the prolongation were recorded in real time (Figure 1b). For the interval from 0 to 60 s, the sampling rate is two samples per second. However, for the interval from 60 to 143 s, the circuit is disconnected, leading to the loop current being zero. In order to accurately measure the length of the precipitated copper, we select the sampling points corresponding to the clear images in the video, and the intervals between two sampling points are not constant.

According to the current vs time and the length vs time curves, the process can be divided into four steps: initial state (c−d), electrochemical extraction (d−g), dynamic equilibrium (g−h), and reverse incorporation (h−l).

During the initial state, the NW is unchanged and the loop current is close to zero. After the first 26 s, the electrochemical extraction (formation of Cu phase) took place quickly, and the length of the formed Cu nanowire reached its maximum at 30 s (Figure 1g). The total current (26−30 s) drastically shoots up to ∼1000 nA. The maximum conductivity of the Cu_2S during the dynamic extrusion state was estimated to be ∼10³
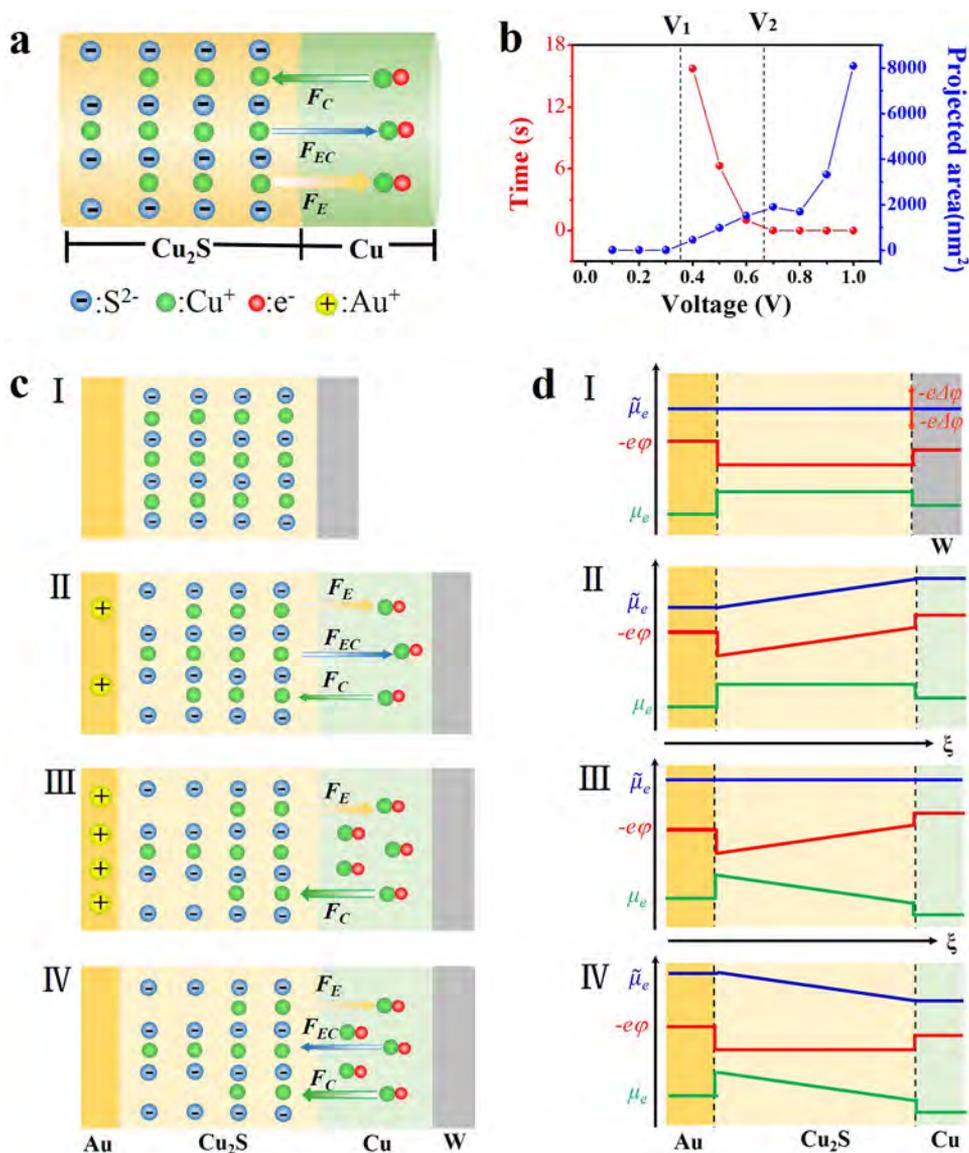
Figure 3. Dynamics of the pseudoelectroelasticity process. (a) Schematic description of the forces acting on the Cu$^+$ ions. The electrochemical driving force (F_{EC}) is a combination of both chemical driving force (F_C) and the electrical driving force (F_E), $F_{EC} = F_E + F_C$. (b) The relaxation time of Cu extrusion and the projected areas of protrusions at 30 s vary with the applied voltages. (c) Schematic diagrams showing the force analysis of four different boundary states in the whole process. (d) Corresponding electron electrochemical potential distribution in the four different states. Electrochemical potential ($\tilde{\mu}$) equals the sum of electrical potential (φ) and chemical potential (μ). The vertical arrows indicate the shift of the equilibrium and the horizontal arrows indicate the direction of the external electric field (ξ).

Siemens/m, consistent with the experiment values reported in the literature[20] (Supporting Information). After this increase, the NW system turned into a dynamic equilibrium state until the end of biasing at 60 s (Figure 1h), the current intensity drops to about several tens of nanoamperes and no further growth of the Cu nanowire was observed. A series of characterizations (Figures S2 and S3) verifying the Cu extraction are included in Supporting Information. After biasing, the electrochemically formed Cu protrusion dissolves back into NW spontaneously in a self-induced way. Meanwhile, the Cu NW is detached from the W tip, and the electric circuit cuts off automatically. The rate of Cu dissolution reduces with time (Figure 1h–l), reflected from the curvature of the length−time dependence curve in Figure 1b. In the end, the protrusion is dissolved almost completely, the shape and the structure of Cu$_2$S NW returned to its initial dimensions

(Figure 1l, Figure S4). The slightly reduced length is caused by the difference of the projection directions.

To understand the detailed migration behavior of Cu$^+$ ions within the Cu$_2$S NW, a series of HRTEM images were recorded, as shown in Figure 2. The corresponding raw HRTEM images are listed in Figures S5 and S6. Starting with biasing the pristine NW for 1.5 s, the LC structure completely turned into HC accompanied by the disappearance of the stacking faults (Figure 2b). The phase transition is caused by Joule heating.[1,18] When constant bias is applied, the Cu$_2$S NW's temperature will rise due to Joule heating until reaching a thermal equilibrium state.[21] We simulated the temperature distribution of a Cu$_2$S NW in thermal equilibrium state by finite element method (Figure S7) and found that the temperature raised by Joule heating is enough to induce phase transition.[1,18] The detailed phase transition path shows

that the phase transformation originates at the stacking faults and propagates from the edge inward until the LC structure is completely converted into HC (Figure S8), which is consistent with our previous work.[18] Subsequently, the Cu atoms begin to nucleate at the tip of the NW (highlighted in green), and the NW maintain the HC phase during the dynamic extrusion process, as shown in Figure 2c and Video S2. The HRTEM image in Figure 2d confirms that the protrusion is entirely made of metallic copper as confirmed from the spacing of the lattice fringes, which agrees with that of {111}-Cu planes. Figure 2e reveals that the $[\bar{1}02]$ diffraction spot of the LC disappears after 1.5 s, which indicates the complete conversion to the HC phase.

The process of Cu reinsertion (Figure 2h−k) is much simpler. With the bias turned off, HC phase converts back to the LC. Surprisingly, the Cu_2S NW keeps LC phase during the entire Cu insertion process as shown in the FFT patterns of Figure 2h−k. It is shown in Figure 2f,g that Cu^+ ions migrate along the c channel in a synchronized way (caterpillar migration) with an energy barrier of less than 0.6 eV. On the contrary, we find that the isolated motion of a single ion along the c channel is not feasible as it encounters huge repulsion from its neighboring ions along the c channel and bounces back to the initial configuration prior to the hop. Combining *in situ* HRTEM observations with *ab initio* calculations, we concluded that the Cu^+ ion diffusion in this case follows the caterpillar diffusion mechanism[22,23] rather than the independent ion motion normally observed in most of the metal−halogen superionic conductors.[1]

The different steps in the deformation process are described a brief manner in Figure 1m. First, the temperature of the Cu_2S NW increases due to Joule heating. Next, a crystallographic phase transition occurs during which, Cu^+ ions in P2 are driven out of their sublattice, replaced by Cu^+ ions from P1. The extruded Cu^+ ions are reduced (precipitate) at the W electrode. These atoms are pushed forward by the newly reduced Cu atoms, and thus the NW is elongated. Once the bias is turned off, the extracted Cu atoms oxidize and move in the reverse direction, back into the NW.

The reversible change both in shape and crystal phase was analogous to the deformation of a nanospring. However, in our case this deformation of NW is excited by electric field rather than by external mechanical force. Despite the complexity of the observed elongation-shortening process, we demonstrate in our work that the extrusion of the Cu NW is an electrically driven process, and that dissolution process is spontaneous. It is worth emphasizing that the process observed in this study is different in nature from other reversible metal extraction-insertion phenomena published hitherto[16,24] (Table S1); for details, see the Supporting Information.

In order to explain the experimental phenomena and the corresponding current curves, we have considered the Au−Cu_2S(Cu)−W structure as solid-state electrochemical system with an ion blocking electrode (Au) and reversible W electrode. In this model (Figure 3a), we assume that the force created by the external electric field acting on Cu^+ ions represents F_E and all the other effects due to the movement of Cu^+ ions are cumulatively included in F_C. On the microscopic level, four discernible states account for the extrusion and insertion of the Cu protrusion as well as the corresponding changes in the distribution of the electrochemical potential of electrons, as illustrated in Figure 3.

Once the Au−Cu_2S−W system is connected, the electrochemical potential $\tilde{\mu}$ of the system equilibrate and the condition $\tilde{\mu}(Au) = \tilde{\mu}(Cu_2S) = \tilde{\mu}(W)$ is fulfilled as shown in Figure 3c(I) and Figure 3d(I). The difference in the work functions of Au and Cu_2S suggest the formation of a Schottky contact at the Au−Cu_2S interface as shown in Figure 3d(I). This is why the initial loop current is close to zero in Figure 1b.

An applied voltage shifts the Fermi level of the Au electrode relative to the Cu_2S ($\Delta E_F(Au) = e\Delta\varphi$) and an effective electrical potential difference ($e\varphi$) is induced, where e is charge of the electron, and φ is the local electrostatic potential. According to the energy band diagram of the Au−Cu_2S−W system (Figure S9), we know that the major potential drop is concentrated between Au and W electrodes as shown by the red line in Figure 3d (II). With external voltage exerted upon the Cu_2S, the mobile Cu^+ ions would respond by moving with a drift mobility, M_d. At the same time, an equal amount of electrons moving from Au electrode to W electrode through the external circuit leads to a formation of positive charges at Au side of the Au/Cu_2S interface. In this way, an electrical double layer is established at the Au/Cu_2S interface to maintain the charge balance of the system. It is the electrical double layer that stabilizes the Cu^+-deficient material. For the electrons arriving at the Cu_2S/W interface from the W electrode with energy (E_I) higher the Fermi energy of the redox reaction, that is, $E_I > E_F$ (Cu^+/Cu), can contribute to the electrochemical Cu^+/Cu half-cell reaction.[12] Meanwhile, the activity of Cu is reduced at the Au/Cu_2S interface (Figure 3c(II)) in accordance to the Nernst equation. The observed high current (Figure 1B) is a proof of the mass/ion transfer in the Cu_2S NW and interface electrode reactions. The ionic conduction is estimated in the order of $\sigma_{ion} = (10-10^2)\sigma_e$ (Supporting Information).

The extraction of Cu from the solid electrolyte will lead to a shift of the chemical potential from the green line in Figure 3d(II) to the green line in Figure 3d(III). When it reaches the level denoted by the green line in Figure 3d(III), an equilibrium will be established as shown in Figure 3c(III). In this case, the chemical potential gradient formed during the application of voltage drives a chemical dissolution process of Cu back into the Cu_2S matrix, and the directional migration of Cu^+ ions stops, so the ionic conduction no longer contributes the loop current. In addition, the extrusion of Cu^+ ions induces cationic vacancies on the Cu_2S side near the Au/Cu_2S interface that provide an additional potential, reducing both the built-in potential and the depletion width to maintain the Fermi energy balance between Au and Cu_2S.[21,25] Therefore, the Schottky barrier at the Au/Cu_2S interface decreases. This is why the current drops to about several tens of nanoamperes during dynamic equilibrium state, which is much smaller than the current in electrochemical extraction process but higher than the current in the initial state.

Upon removal of bias, the extracted Cu starts to be oxidized and dissolved back into the NW, driven by chemical potential gradient (higher copper concentration toward the W tip side), as shown in Figure 3c(IV). The Cu species will gradually become uniformly spanned inside the NW again, and the chemical potential distribution is shifted from the green line in Figure 3d(IV) to the green line in Figure 3d(I). Obviously, the dissolution of Cu protrusion is slower than the growth, which is because of the electronic conductivity is smaller than the ionic conductivity in Cu_2S in Figure 1b. During electrochemical extraction process, the Cu^+ ions diffusion through
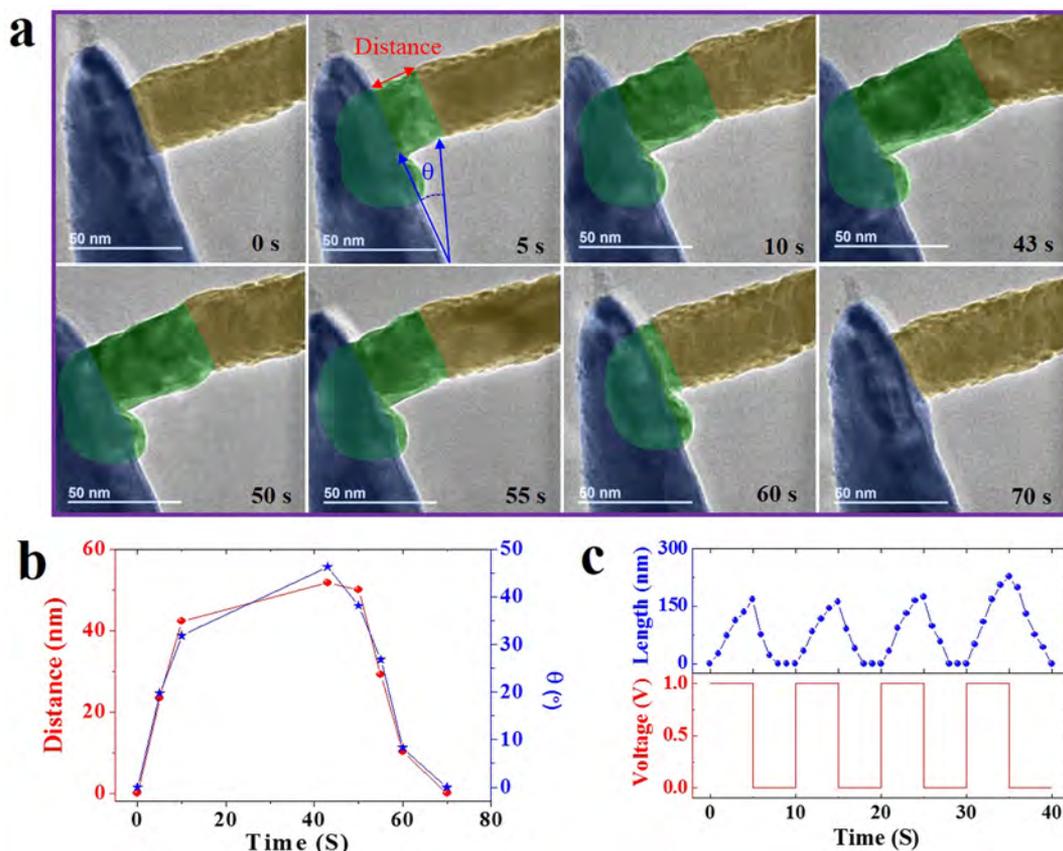
Figure 4. Single nanowire electric nanoactuator. (a) Sequential images showing the whole process of a Cu$_2$S nanoactuator. During 1 V biasing, the W tip is pushed away by the protrusion formed by extruded Cu. After biasing, the Cu$_2$S NW constricts spontaneously and the W tip returns to its original position (Video S3). So the Cu$_2$S NW can be used as a nanoactuator to drive reciprocating motion of an object. The golden color highlights the Cu$_2$S; the green color highlights Cu protrusion and the blue color highlights W tip. (b) Change in the relative distance marked by red two-way arrow (from W tip to Cu/Cu$_2$S interface) and angle θ marked by two blue arrows in part a during the pseudoelectroelasticity process. (c) Repeatability of a nanoactuator behavior.

Cu$_2$S NW and the electrons transfer through the external circuit, so the Cu protrusion formation process is ionic conduction limiting.[5] However, for the Cu dissolution process, the electric circuit cuts off after bias, so electrons only can transfer through Cu$_2$S NW, and the Cu protrusion dissolution process becomes electronic conduction limiting.[5]

The value of the applied voltage also influences the process of Cu extraction (Figure S10). Constant voltages of variable amplitudes (0−1 V, the interval is 0.1 V) were applied on the NW, the time of Cu$^+$ ions to begin moving out and the projected areas of Cu protrusions at 30 s were recorded as shown in Figure 3b. On the basis of these data, the phenomenon of pseudoelectroelasticity can be divided into three categories. It is worth mentioning that the voltage ranges of these three categories varied for different NWs. For a specific NW, the process of Cu$^+$ ion precipitation has two critical voltages V_1 and V_2 (Figure 3b). There is a positive correlation between the temperature and the applied voltage, since increasing the applied voltage will raise the steady-state temperature of the NW. If the bias is below V_1, the electric force on the ion is not sufficient to overcome the Cu$^+$ ion reduction and diffusion barriers in LC Cu$_2$S and also, the steady-state temperature of the NW is below the phase transition temperature, which means that the Cu$^+$ ions will not precipitate out of the NW. When the bias is between V_1 and V_2, the electrical field, in this case, is also not sufficient to

overcome the Cu$^+$ ion reduction/diffusion barrier in LC Cu$_2$S, but the steady-state temperature of the NW can increase to above the phase transition temperature, in which case, Cu$^+$ ions can become mobile in HC Cu$_2$S. Thus, the relaxation time required to induce precipitation of Cu$^+$ ions reduces with increasing applied voltage. The measured projected areas of the Cu protrusions at 30 s increase with voltage in this range of applied voltage (Figure S10b−d). Above V_2, the electrical field force is sufficient to overcome the Cu$^+$ ion reaction/diffusion barriers in LC Cu$_2$S and Cu ions instantaneously are electrochemically extracted from the NW following applied bias. In this case, the projected area of the Cu protrusions at 30 s increases with voltage except for 0.8 V, because the protrusion is overlapped in Figure S10f.

Last, we demonstrate the use of the pseudoelectroelasticity behavior of Cu$_2$S in a linear electric nanoactuator (Figure 4). In this way, we can directly convert electrical energy into mechanical energy, which can be used to drive the reciprocating motion of an object (Video S3). We chose the interface of Cu/Cu$_2$S interface of the NW as reference position. At a bias of 1 V, the Cu$^+$ ions move out and push the W tip out. If the bias is turned off, the extruded Cu$^+$ inserts back into the NW and pulls the W tip to its original location (Figure 4a). The relative positions and the relative change in the orientation of the W tip are presented in Figure 4b. We have repeated the actuation process many times for another

NW and found that the movement of the nanoactuator was precisely repeated, confirming the reliability of the system (Figure 4c and Video S4).

Conclusion. In summary, we directly monitored the pseudoelectroelasticity process of Cu_2S NWs at the atomic scale and have successfully applied this mechanism to nanoelectromechanical systems. The details of the electrochemical dynamics are revealed, which include Cu_2S phase transformation, migration and jamming of Cu^+ ions, nucleation, growth, as well as spontaneous shrinking of Cu protrusion. The microscopic mechanism convincingly demonstrates that the extraction of Cu^+ ions is driven by the external electric field and the cation diffusion barriers are dominated by Joule heat, whereas the oxidation and reinsertion of Cu in the absence of bias is due to the chemical potential difference. Our results open a new perspective about the properties of superionic conductor and provide critical insight into the microscopic mechanisms of ion transport, thereby motivating further research to broaden this concept in electrochemical and nanoelectromechanical systems.

◼ ASSOCIATED CONTENT

Ⓢ Supporting Information

The Supporting Information is available free of charge on the ACS Publications website at DOI: 10.1021/acs.nano-lett.8b01914.

> Synthesis of copper(I) sulfide NWs, set up of the *in situ* TEM experiment, characterization method and electrical measurements, first-principles calculations, simulation of temperature gradient, conductivity measurements, determination of the structure of the protrusion formed under bias, and the source of extruded Cu ions; figures including structural characterization and elemental composition of samples and the protrusion, the raw HRTEM images corresponding to Figure 2, temperature distribution of Cu_2S NW, the phase transition trajectory from LC to HC during the extrusion process, the energy band diagram of the $Au/Cu_2S/W$ structure, and the influence of voltage on the Cu extrusion process; and Table S1, showing the analysis of device structure, elasticity or plasticity, dominant ions source, position of extrusion, and dominant driving force in different kinds of reversible metal extrusion-insertion processes(PDF)
>
> Video S1, electric field induced pseudoelectroelasticity deformation of one Cu_2S nanowire, where the extrusion of the Cu NW is an electrically driven process and that dissolution process is spontaneous (AVI)
>
> Video S2, extrusion process of the Cu NW at high resolution (AVI)
>
> Video S3, one Cu_2S nanowire working as a nanoactuator to drive reciprocating motion of an object (here is W tip) (AVI)
>
> Video S4, repeatability of a nanoactuator behavior (AVI)

◼ AUTHOR INFORMATION

Corresponding Authors

*(L.S.) E-mail: slt@seu.edu.cn.
*(Ha.Z.) E-mail: hmzheng@lbl.gov.
*(I.V.) E-mail: i.valov@fz-juelich.de.

ORCID Ⓞ

Ilia Valov: 0000-0002-0728-7214
Haimei Zheng: 0000-0003-3813-4170
Litao Sun: 0000-0002-2750-5004

◼ ABBREVIATIONS

Cu_2S, copper sulfide; HRTEM, high resolution transmission electron microscope; STM-TEM, scanning tunneling microscopic-transmission electron microscope system; HC, high chalcocite; LC, low chalcocite; NW, nanowire; SAED, selected area electron diffraction; EELS, energy-loss spectroscopy; FFT, fast Fourier transformation; NEB, nudged elastic band

◼ REFERENCES

(1) Wang, L.-W. *Phys. Rev. Lett.* **2012**, *108* (8), 085703.
(2) Morcrette, M.; Rozier, P.; Dupont, L.; Mugnier, E.; Sannier, L.; Galy, J.; Tarascon, J. M. *Nat. Mater.* **2003**, *2* (11), 755−61.
(3) Liu, H.; Shi, X.; Xu, F.; Zhang, L.; Zhang, W.; Chen, L.; Li, Q.; Uher, C.; Day, T.; Snyder, G. J. *Nat. Mater.* **2012**, *11* (5), 422−5.
(4) He, Y.; Day, T.; Zhang, T.; Liu, H.; Shi, X.; Chen, L.; Snyder, G. J. *Adv. Mater.* **2014**, *26* (23), 3974−8.
(5) Chen, C. C.; Fu, L.; Maier, J. *Nature* **2016**, *536* (7615), 159−64.
(6) Ohno, T.; Hasegawa, T.; Tsuruoka, T.; Terabe, K.; Gimzewski, J. K.; Aono, M. *Nat. Mater.* **2011**, *10* (8), 591−5.
(7) Aoki, Y.; Wiemann, C.; Feyer, V.; Kim, H. S.; Schneider, C. M.; Ill-Yoo, H.; Martin, M. *Nat. Commun.* **2014**, *5*, 3473.
(8) Wang, J.; Chen, K.; Gong, M.; Xu, B.; Yang, Q. *Nano Lett.* **2013**, *13* (9), 3996−4000.
(9) Terabe, K.; Hasegawa, T.; Nakayama, T.; Aono, M. *Nature* **2005**, *433* (7021), 47−50.
(10) Maier, J. *Nat. Mater.* **2005**, *4* (11), 805−815.
(11) Sata, N.; Eberman, K.; Eberl, K.; Maier, J. *Nature* **2000**, *408* (6815), 946−949.
(12) Valov, I.; Sapezanskaia, I.; Nayak, A.; Tsuruoka, T.; Bredow, T.; Hasegawa, T.; Staikov, G.; Aono, M.; Waser, R. *Nat. Mater.* **2012**, *11* (6), 530−5.
(13) Wedig, A.; Luebben, M.; Cho, D. Y.; Moors, M.; Skaja, K.; Rana, V.; Hasegawa, T.; Adepalli, K. K.; Yildiz, B.; Waser, R.; Valov, I. *Nat. Nanotechnol.* **2016**, *11* (1), 67−74.
(14) Nayak, A.; Tamura, T.; Tsuruoka, T.; Terabe, K.; Hosaka, S.; Hasegawa, T.; Aono, M. *J. Phys. Chem. Lett.* **2010**, *1* (3), 604−608.
(15) Xu, Z.; Bando, Y.; Wang, W.; Bai, X.; Golberg, D. *ACS Nano* **2010**, *4* (5), 2515−2522.

(16) McDowell, M. T.; Lu, Z.; Koski, K. J.; Yu, J. H.; Zheng, G.; Cui, Y. *Nano Lett.* **2015**, *15* (2), 1264−1271.

(17) Nayak, A.; Tsuruoka, T.; Terabe, K.; Hasegawa, T.; Aono, M. *Nanotechnology* **2011**, *22* (23), 235201.

(18) Zheng, H.; Rivest, J. B.; Miller, T. A.; Sadtler, B.; Lindenberg, A.; Toney, M. F.; Wang, L. W.; Kisielowski, C.; Alivisatos, A. P. *Science* **2011**, *333* (6039), 206−209.

(19) Rivest, J. B.; Fong, L.-K.; Jain, P. K.; Toney, M. F.; Alivisatos, A. P. *J. Phys. Chem. Lett.* **2011**, *2* (19), 2402−2406.

(20) Okamoto, K.; Kawai, S. *Jpn. J. Appl. Phys.* **1973**, *12* (8), 1130.

(21) Zhang, Q.; Yin, K.; Dong, H.; Zhou, Y.; Tan, X.; Yu, K.; Hu, X.; Xu, T.; Zhu, C.; Xia, W. *Nat. Commun.* **2017**, *8*, 14889.

(22) Yokota, I. *J. Phys. Soc. Jpn.* **1966**, *21* (3), 420−423.

(23) He, X.; Zhu, Y.; Mo, Y. *Nat. Commun.* **2017**, *8*, 15893.

(24) Zhang, C.; Cretu, O.; Kvashnin, D. G.; Kawamoto, N.; Mitome, M.; Wang, X.; Bando, Y.; Sorokin, P. B.; Golberg, D. *Nano Lett.* **2016**, *16* (10), 6008−6013.

(25) Yan, Z.; Liu, J.-M. *Sci. Rep.* **2013**, *3*, 02482.